Alteration of Water Exchange Rates Following Focused Ultrasound-Mediated BBB Opening in the Dorsal Striatum of Non-Human Primates: A Diffusion-Prepared pCASL Study

Dong Liu[a,b*], Xingfeng Shao[c], Fabian Munoz Silva[a,b], Soroosh Sanatkhani[a,b], Ray Lee[d], Elisa E Konofagou [e,f], Danny JJ Wang [c], Vincent P Ferrera [a,b,g]

[a] Dept. of Neuroscience, Columbia University, New York, NY, USA

[b] Zuckerman Mind Brain Behavior Institute, Columbia University, New York, NY, USA

[c] Stevens Neuroimaging and Informatics Institute, Keck School of Medicine, University of Southern California, Los Angeles, CA, USA

[d] Dept. of Radiology, University of Texas Health Science Center at San Antonio, San Antonio, TX, USA

[e] Dept. of Biomedical Engineering, Columbia University, New York, NY, USA

[f] Dept. of Radiology, Columbia University, New York, NY, USA

[g] Dept. of Psychiatry, Columbia University, New York, NY, USA

*dl3341@columbia.edu

Abstract

This study applied diffusion-prepared pseudo-continuous arterial spin labeling (DP-pCASL) to quantify cerebral blood flow (CBF), arterial transit time (ATT), and blood-brain barrier (BBB) water exchange rate (K_w) before and after focused ultrasound (FUS)-mediated blood-brain barrier opening (BBBO) in the dorsal striatum of four non-human primates. Six baseline and seven BBBO sessions were performed. DP-pCASL was acquired approximately 45 minutes after FUS sonication combined with intravenous microbubbles, and contrast-enhanced T1-weighted imaging was subsequently used to confirm the BBBO region. Whole-brain analyses revealed no significant changes in CBF or ATT following BBBO (permutation $p > 0.05$). Region-of-interest analysis within the sonicated caudate demonstrated a significant localized decrease in K_w, with median (IQR) values of 45.0 (40.6 - 55.6) min^{-1} at the BBBO site versus 61.6 (58.3 - 70.4) min^{-1} in the contralateral control region ($p < 0.05$), confirming spatially specific suppression of transendothelial water flux. In contrast, whole-brain K_w increased significantly following BBBO, with median (IQR) values of 49.8 (46.3 - 55.9) min^{-1} in non-BBBO sessions versus 59.4 (56.6 - 66.3) min^{-1} in BBBO sessions ($p < 0.01$), indicating a diffuse enhancement of water exchange across the brain. These findings establish DP-pCASL-derived K_w as a sensitive, non-contrast biomarker for both local and global BBB permeability changes induced by focused ultrasound, supporting its potential for longitudinal monitoring in preclinical and clinical neurotherapeutic applications.

Introduction

Focused ultrasound (FUS) combined with intravenously administered microbubbles enables a safe, transient, and localized opening of the blood-brain barrier (BBB) (Aryal et al., 2014; Hynynen et al., 2001; McDannold et al., 2007). This effect is achieved by applying focused acoustic energy that causes circulating microbubbles within targeted cerebral vessels to oscillate(Marquet et al., 2014; Tung et al., 2011), generating mechanical forces that temporarily disrupt endothelial tight junctions (Konofagou, 2012; Sheikov et al., 2004). By temporarily disrupting the BBB, FUS facilitates the delivery of therapeutic agents such as chemotherapeutic drugs, antibodies, and viral vectors into selected brain regions, offering promising treatments for neurological and psychiatric disorders including Alzheimer's disease, Parkinson's disease, and brain cancers (Leinenga et al., 2016; Lipsman et al., 2018; Mainprize et al., 2019; Rezai et al., 2020). While these agents primarily penetrate the brain via paracellular diffusion through the disrupted tight junctions, additional pathways such as receptor-mediated transcytosis and adsorptive endocytosis may also facilitate their transport (Burgess et al., 2015; Hawkins and Davis, 2005). Similarly, gadolinium-based contrast agents, which normally cannot cross an intact BBB, gain access through these temporary junctional openings and accumulate in brain tissue. This characteristic underpins the use of gadolinium-enhanced magnetic resonance imaging (MRI) as the standard method for detecting and confirming BBB opening in both research and clinical settings (McDannold et al., 2006). However, concerns regarding the safety of repeated gadolinium administration, including risks of nephrogenic systemic fibrosis and gadolinium retention in brain tissue, have prompted the development of contrast-free imaging methods to safely monitor BBB integrity over repeated treatments (Gulani et al., 2017; Kanda et al., 2014).

In addition to facilitating molecular delivery, focused ultrasound-induced BBB opening (FUS-BBBO) can modulate neural activity, triggering significant changes in brain functional connectivity

and neuroinflammation, as well as influencing behavior outcomes. For instance, studies in non-human primates have reported enhanced cognitive performance, including improved response speed and accuracy, following targeted striatal FUS-BBBO, indicating neuromodulatory effects beyond simple molecular delivery (Chu et al., 2015; Pouliopoulos et al., 2021; Todd et al., 2019). Functional MRI studies have demonstrated that FUS-BBBO can alter resting-state functional connectivity in both animals and humans, suggesting transient disruption of network dynamics (Meng et al., 2019; Todd et al., 2018). Notably, a recent non-human primate study compared the effects of FUS-neuromodulation and FUS-BBBO, showing that BBB opening alone can induce robust, region-specific changes in connectivity, further supporting a neuromodulatory role that does not depend on drug delivery (Liu et al., 2023). In parallel, FUS-BBBO has been shown to elicit transient neuroinflammatory responses, including glial activation, which may further contribute to downstream plasticity and behavioral effects (Kovacs et al., 2017; McMahon and Hynynen, 2017). Despite accumulating evidence of these neuromodulatory phenomena, the precise physiological mechanisms underlying these broader effects remain incompletely understood, necessitating deeper exploration into the cellular, molecular, and functional changes triggered by transient FUS-BBBO.

A key factor in maintaining neurovascular homeostasis, which may potentially be involved in the neuromodulatory effects of FUS-BBBO, is the regulation of water transport across the BBB. Aquaporin-4 (AQP4), a water channel protein abundantly expressed on astrocytic endfeet at the gliovascular interface, facilitates water exchange in response to osmotic and hydrostatic gradients, modulating cerebral edema, neuroinflammation, and glymphatic clearance (Papadopoulos and Verkman, 2013). Given its small molecular size (~18 Da), water acts as a highly sensitive endogenous tracer, capable of detecting subtle permeability alterations that larger molecules such as gadolinium (~550 Da) might fail to reveal (Dickie et al., 2020; Shao et al., 2020; Uchida et al., 2023). Thus, studying water transport dynamics offers an exceptionally sensitive and

physiologically relevant avenue to detect and better understand subtle BBB permeability and functional changes induced by FUS-BBBO.

Diffusion-prepared pseudo-continuous arterial spin labeling (DP-pCASL) is a recently developed, non-invasive MRI technique to quantify the water exchange rate (K_w) across the BBB. By combining diffusion weighting with ASL and employing multi-post-labeling delay acquisitions, DP-pCASL improves K_w accuracy by accounting for arterial transit time (ATT) variability (Shao et al., 2019; St. Lawrence et al., 2012; Wang et al., 2007). Clinical studies have reported changes of BBB K_w in association with aging (Shao et al., 2024) and various neurological conditions, including multiple sclerosis (Wengler et al., 2020), obstructive sleep apnea (Palomares et al., 2015) and cerebral small vessel disease (Li et al., 2023). In Alzheimer's disease, Chen et al. reported significantly reduced K_w in the hippocampus, cingulate cortex, and other brain regions, with associations to plasma biomarkers and cognitive performance, suggesting K_w as a promising biomarker for early BBB dysfunction (Chen et al., 2025). Additionally, Tiwari et al. (2025) demonstrated the sensitivity of diffusion-weighted ASL MRI to mannitol-induced BBB disruption in rodents, validated by contrast-enhanced MRI and histology (Tiwari et al., 2025).

Despite these methodological advancements, DP-pCASL has not yet been applied to characterize the changes in water exchange dynamics associated with FUS-induced BBB opening. The aim of the present study, therefore, is to quantify alterations in cerebral blood flow (CBF) and BBB water exchange rate (K_w) following FUS-BBBO targeting the dorsal striatum of non-human primates (NHPs) (**Figure 1**). By directly comparing these gadolinium-free DP-pCASL measures with conventional gadolinium-enhanced MRI, we seek to evaluate the potential of DP-pCASL as a non-contrast imaging approach for assessing BBB permeability and to gain insight into the mechanisms by which focused ultrasound transiently alters BBB integrity.

Materials and Methods

Animal Preparation

Four adult male NHPs, 2 long-tailed macaques (*Macaca fascicularis*) and 2 rhesus macaques (*Macaca mulatta*), weighing between 7.1 and 14.1 kg, were included in this study. Prior to the ultrasound and MRI procedures, animals were initially sedated with ketamine (10 mg/kg) and dexmedetomidine (0.02 mg/kg). Anesthesia was then maintained with inhaled isoflurane at concentrations ranging from 0.8% to 1.1% throughout the experiments. The scalp hair was shaved, and a conductive gel was applied to optimize acoustic coupling for ultrasound delivery. During MRI scanning, physiological parameters—including body temperature, electrocardiogram, oxygen saturation, and end-tidal CO_2—were continuously monitored using a wireless MRI-compatible system (Iradimed 3880). All experimental protocols were conducted in accordance with guidelines approved by the Institutional Animal Care and Use Committee (IACUC) of Columbia University.

FUS with microbubbles application

A single-element FUS transducer (model H-107; 500 kHz frequency; radius of curvature 63.2 mm; outer diameter 64 mm; Sonic Concepts, Bothell, WA) was used for all sonication. The transducer was driven by a function generator (Agilent 33220A, Agilent Technologies, Santa Clara, CA) connected to a 57 dB radiofrequency power amplifier (500S06, E&I, Rochester, NY). The transducer's acoustic output was calibrated in a degassed water tank using a capsule hydrophone (HGL-0200, Onda Corp., Sunnyvale, CA), which measured free-field pressure, focal location, and acoustic intensities including spatial-peak pulse average (I_{sppa}) and spatial-peak temporal average (I_{spta}). To estimate the actual acoustic pressure reaching the brain, attenuation through *ex vivo*

NHP skulls was measured. In this study, we assumed an approximately 65% reduction in acoustic pressure due to the skull and used the derated peak negative pressure (PNP), which incorporates this attenuation, to report sonication parameters.

On the day of MRI scanning, the transducer cone was filled with degassed water using a WDS105+ water degassing system (Sonic Concepts, Bothell, WA) and attached securely to the NHP's scalp to optimize ultrasound transmission. Sonication parameters were based on established protocols to safely and effectively induce BBB opening in NHPs. Animals received sonication for 2 minutes at a derated PNP of 400 kPa, with a pulse repetition frequency (PRF) of 2 Hz, pulse duration of 10 ms, and a 2% duty cycle, as illustrated in **Figure 2**. In-house manufactured microbubbles (diameter 4–5 μm; concentration 2.5×10^8 bubbles/kg) were administered intravenously via the saphenous vein approximately 10 seconds after the start of sonication. The spatial peak temporal average intensity (Ispta) for BBB opening was 39.2 mW/cm^2. This ultrasound intensity was selected to reliably open the BBB while maintaining safety, as supported by prior studies(Liu et al., 2023; Pouliopoulos et al., 2021).

MRI Acquisition

MRI data were acquired on a 3T Siemens Prisma scanner using a 15-channel knee coil optimized for imaging the NHP brain, and the detailed MRI timeline is shown in **Figure 2**. Structural T1-weighted images were obtained using a T1-MPRAGE sequence with the following parameters: repetition time (TR) = 2580 ms, echo time (TE) = 2.81 ms, inversion time (TI) = 1160 ms, flip angle (FA) = 9°, isotropic resolution of 0.5 mm^3, and field of view (FOV) = 128 × 128 × 120 mm^3.

DP-pCASL with background-suppressed 3D gradient-and-spin-echo (GRASE) readout was performed within 45 minutes after FUS sonication to measure ATT, CBF, and the BBB K_w,

following a protocol similar to that described by Shao et al. (Shao et al., 2019). The detailed parameters included: field of view (FOV) = 138 mm, matrix size = 64 × 64, 14 axial slices, voxel size = 2.2 × 2.2 × 5 mm^3, turbo factor = 14, EPI factor = 64, bandwidth = 2232 Hz/pixel, TE = 31.84 ms, TR = 3200 ms, labeling/control duration = 1000 ms, labeling offset = 55 mm, and centric k-space ordering. Multiple post-labeling delays (PLDs) (600, 1400 and 1700 ms) were acquired with diffusion weightings (b-values) applied to capture water exchange dynamics.

To confirm FUS-mediated BBBO, T1-weighted images were acquired using a T1-SPACE protocol, selected for its sensitivity to low gadolinium concentrations (Danieli et al., 2019), within 20 minutes following intravenous administration of gadolinium-based contrast agent at a dose of 0.2 mmol/kg. The T1-SPACE images matched the pre-contrast T1 and resolution to enable direct comparison.

MR Image Analysis

A two-stage estimation approach was used to quantify CBF, ATT and BBB K_w from perfusion images acquired at specific post-labeling delays (PLD) and diffusion weightings (b-values) (St. Lawrence et al., 2012), as described in **Figure 3**. In the first stage, ATT was estimated using the flow-encoding arterial spin tagging (FEAST) method, calculated from the ratio of vascular-suppressed signals (with diffusion weighting = 10 s/mm^2 and velocity encoding [VENC] = 7.5 mm/s) to the total perfusion signals acquired at a short PLD of 600 ms (Wang et al., 2003). In the second stage, K_w was calculated by fitting data acquired at two longer PLDs of 1,400 ms and 1,700 ms with diffusion weightings of b = 0 and 25 s/mm^2, which allows separation of vascular and extravascular compartments using a two-compartment single-pass approximation (SPA) model (Shao et al., 2019; St. Lawrence et al., 2012). CBF was computed from perfusion signals measured at PLD = 1,700 ms without diffusion weighting (Alsop et al., 2015).

Whole-brain average values of CBF, ATT, and K_w were computed by generating voxel-wise parametric maps for each metric and then averaging across all intracranial voxels within a manually created NHP brain mask for each session. Comparisons between non-BBBO (n = 6) and BBBO (n = 7) whole-brain averages used two-tailed independent-samples permutation tests (10 000 iterations) in MATLAB R2023a (The MathWorks, Natick, MA, USA), with mean difference (Δ), p-value, and Hedges' g reported.

Regions of interest (ROIs) were manually delineated on the parametric maps at the axial slice intersecting the dorsal striatum, with a T1-weighted scan acquired at the same slice plane used to confirm the sonication target region. Each ROI covered a 2 × 2 × 1 voxel volume (4.4 × 4.4 × 5 mm^3) and was mirrored to the contralateral hemisphere for within-subject comparison. Paired-sample permutation testing (10,000 iterations) in MATLAB was used to compare ROI values between BBBO and contralateral control regions. All co-registration of structural images to parametric maps and ROI drawing were performed in FSL v6.0 (FMRIB Software Library, University of Oxford, Oxford, UK) (Jenkinson et al., 2012). Statistical significance was defined at $p < 0.05$.

Results

Mapping of CBF, ATT, and K_w and its relation to contrast-enhanced T1

We first tested the effect of FUS-BBBO on hemodynamics and BBB water exchange. **Figure 4A** shows voxel-wise maps of CBF, ATT, and BBB K_w in the axial plane through the dorsal striatum for two representative BBBO sessions in NHPs T and R. Both sessions targeted the right caudate and were acquired immediately after sonication with microbubbles. The CBF maps illustrate the baseline perfusion pattern throughout the striatum, with no systematic ipsilateral-to-contralateral

differences attributable to BBBO. ATT maps display considerable variability across individual sessions, with average ATT values ranged from 918 to 1288 ms; however, there is no clear spatial correspondence between ATT heterogeneity and the BBBO locus. By contrast, K_w maps reveal pronounced, spatially restricted reductions in water-exchange rate at or immediately adjacent to the sonication site (white arrows), highlighting the unique sensitivity of K_w to focal BBB permeability changes.

In **Figure 4B**, we highlight two independent examples—one BBBO in the right caudate and one in the left caudate—by first normalizing each K_w map to its maximum value across the entire brain and then overlaying the interpolated results on post-gadolinium T_1-weighted images, which delineate regions of contrast uptake. In both examples, K_w at the sonication locus reduced by approximately 15–40 % compared to the contralateral hemisphere, providing clear visual and quantitative confirmation that DP-pCASL–derived decreases in K_w co-localize with contrast-verified BBB openings. This dual-modal mapping underscores the high spatial specificity of K_w as a biomarker for localized BBB disruption following FUS-BBBO.

Group-level comparison of whole-brain averages

To assess the reproducibility of BBBO effects, whole-brain CBF, ATT, and K_w were compared across four NHPs (non-BBBO: 6 sessions; BBBO: 7 sessions) via non-parametric permutation tests (**Figure 5A**). Whole-brain CBF showed no significant change following BBBO, with median (IQR) values of 31.3 (22.5–36.5) $\mathrm{ml} \cdot 100\ \mathrm{g}^{-1} \cdot \mathrm{min}^{-1}$ in non-BBBO versus 29.3 (22.2–33.0) $\mathrm{ml} \cdot 100\ \mathrm{g}^{-1} \cdot \mathrm{min}^{-1}$ in BBBO; permutation testing (10 000 iterations) yielded p = 0.64, a mean Δ = -3.0 $\mathrm{ml} \cdot 100\ \mathrm{g}^{-1} \cdot \mathrm{min}^{-1}$, and Hedges' g = -0.25. Whole-brain ATT shifted from a median (IQR) of 1204 (931–1264) ms in non-BBBO to 989 (930–1042) ms in BBBO; despite this apparent decrease, permutation testing (10 000 iterations) indicated no significant effect (p = 0.22; mean Δ

= -106.9 ms; Hedges' g = -0.65). In contrast, whole-brain K_w increased significantly after BBBO, with median (IQR) values of 49.8 (46.3 - 55.9) min^{-1} in non-BBBO versus 59.4 (56.6 - 66.3) min^{-1} in BBBO; permutation testing (10, 000 iterations) yielded p < 0.01, a mean Δ = 13.6 min^{-1} and Hedges' g = 1.46, indicating a diffuse enhancement of water-exchange rate across the brain.

ROI analysis between BBBO site and contralateral control

To assess focal effects of BBBO, CBF, ATT, and K_w were compared within the caudate ROI at the BBBO site versus the mirrored contralateral control (n = 7 sessions) using two-tailed paired permutation tests (10,000 iterations; **Figure 5B**). CBF showed no significant change following BBBO, with median values of 31.3 (24.7- 32.0) $\mathrm{ml} \cdot 100\,\mathrm{g}^{-1} \cdot \mathrm{min}^{-1}$ in the contralateral control versus 32.0 (29.3 – 34.7) $\mathrm{ml} \cdot 100\,\mathrm{g}^{-1} \cdot \mathrm{min}^{-1}$ in the BBBO ROI; permutation testing yielded p = 0.46, a mean Δ = 3.4 $\mathrm{ml} \cdot 100\,\mathrm{g}^{-1} \cdot \mathrm{min}^{-1}$, and Hedges' g = 0.27. ATT likewise showed no significant change, with median values of 1034.9 (972.5 – 1131.5) ms in control versus 989.6 (887.9 - 1120.9) ms in BBBO (p = 0.58; mean Δ = -30 ms; Hedges' g = -0.17). K_w decreased significantly at the BBBO site, with median values of 61.6 (58.3 – 70.4) min^{-1} in control versus 45.0 (40.6 – 55.6) min^{-1} in BBBO; permutation testing yielded p < 0.05, a mean Δ = -15.7 min^{-1} and Hedges' g = -1.51, indicating a localized suppression of water-exchange rate at the sonication locus.

Discussion

This study demonstrates that FUS combined with microbubbles significantly reduces BBB K_w in the dorsal striatum of non-human primates. By contrast, our between-group analysis showed that whole-brain K_w was significantly higher in BBBO cases than in non-BBBO controls. The local reduction in K_w is consistent with a recent rodent study by Tiwari et al. (Tiwari et al., 2025), which used diffusion-weighted ASL MRI to assess BBB water exchange following chemically induced disruption and reported significantly reduced K_w in the affected hemisphere. Similar reductions in K_w have also been reported in individuals with neurological conditions such as aging, Alzheimer's disease, and cerebrovascular disorders, where impaired BBB function has been frequently reported. (Chen et al., 2025; Palomares et al., 2015; Uchida et al., 2023; Wengler et al., 2020). Together, these converging results suggest that reduced K_w may serve as a common physiological signature of compromised BBB function, whether induced by external interventions or underlying disease, and support its application in evaluating the impact of FUS-BBBO.

The focal reduction in BBB K_w observed after FUS-BBBO suggests underlying cellular and molecular adaptations in response to barrier disruption. Aquaporin-4 (AQP4) water channels, primarily located on astrocytic endfeet, are key regulators of cerebral water homeostasis and glymphatic clearance (Mestre et al., 2018; Papadopoulos and Verkman, 2013). FUS-induced loosening or disruption of tight junctions may activate signaling pathways that alter AQP4 expression or polarization—potentially as a protective mechanism to regulate transvascular water flux and limit vasogenic edema (Cong and Kong, 2020). Similar regulatory responses have been reported in neuropathological conditions associated with BBB dysfunction, such as Alzheimer's disease, stroke, and traumatic brain injury (Hirt et al., 2017; Tang et al., 2014; Zeppenfeld et al., 2017). Therefore, a reduction in K_w at the FUS-sonicated area may reflect an active homeostatic adjustment rather than a passive increase in permeability or leakage.

Moreover, our studies align with a growing consensus that BBB permeability is a dynamic, multifactorial phenomenon rather than a mere consequence of tight-junction disruption (Daneman and Prat, 2015; Sweeney et al., 2018). Endothelial remodeling, including changes in cell shape, junctional protein expression and transporter activity, pericyte detachment or loss, and astrocyte endfoot reactivity all modulate paracellular and transcellular flux (Abbott et al., 2006; Armulik et al., 2011). In parallel, neuroinflammatory mediators (e.g. IL-1β, TNF-α, matrix metalloproteinases, reactive oxygen species) and glymphatic flow disturbances each contribute to net water and solute exchange across the barrier (Kovacs et al., 2017; Mestre et al., 2018). By capturing the rapid FUS-induced changes in BBB K_w of non-human primates, DP-pCASL provides a single quantitative measure that integrates the net effects of endothelial remodeling, astrocyte reactivity, and inflammatory signaling on BBB water exchange (Kovacs et al., 2017; Shao et al., 2019).

In this study, we also observed a significant increase in the whole-brain K_w following FUS-BBBO targeted to the caudate nucleus. While the underlying mechanism remains unclear, a recent study has linked elevated whole brain K_w to improved executive function in older adults (Pappas et al., 2024). Although our study did not directly assess cognitive function after BBBO, earlier work has shown that FUS-BBBO can enhance visual behavior task performance in non-human primates by improving both accuracy and response speed, suggesting a potential neuromodulatory effect accompanying BBBO (Chu et al., 2015; Downs et al., 2017). Furthermore, recent work has demonstrated that FUS-BBBO in the dorsal striatum can activate broader brain networks including the default mode network and frontotemporal network (Liu et al., 2023). These findings raise the possibility that global K_w increases may reflect broader functional shifts in neurovascular regulation or fluid transport pathways beyond the sonicated target.

This study also investigates the potential of DP-pCASL as a non-invasive, contrast-free imaging biomarker for monitoring FUS-induced BBB permeability. Currently, dynamic contrast enhanced MRI (DCE-MRI) is widely used to evaluate BBB integrity by measuring the leakage of contrast

agents (CA) into the tissue's interstitial space, indicated by increased T1-weighted signal intensity. Using pharmacokinetic model computations, the volume transfers constant K^{trans} serves as a surrogate measure of BBB permeability (Sourbron and Buckley, 2013). However, the safety of exogenous parametric CA (i.e. Gadolinium) has become a concern for human health (Gulani et al., 2017; Harvey et al., 2020). Recent research has focused on non-Gd-based methods for imaging the BBB integrity, including the use of D-glucose as a CA for chemical exchange saturation transfer (CEST) MRI (Xu et al., 2015), and arterial spin labeling (ASL) for measuring water exchange as a marker for non-contrast detection of BBB impairment (Li et al., 2022). Diffusion tensor imaging (DTI) has been investigated as a non-contrast method for BBB opening detection, linking changes in fractional anisotropy to BBB permeability (Karakatsani et al., 2020). However, DTI provides no direct hemodynamic or perfusion metrics, such as cerebral blood flow or volume, that are more physiologically tied to barrier function (Le Bihan and Iima, 2015). In contrast, DP-pCASL specifically quantifies BBB water exchange rates by differentiating labeled water in vascular and extravascular compartments using diffusion weighting and kinetic modeling(Shao et al., 2019; St. Lawrence et al., 2012). This provides a direct and physiologically meaningful measurement of BBB permeability to water, an endogenous tracer with small molecular size and ubiquitous presence.

This study did not reveal sustained or statistically significant changes in CBF or ATT at either the whole-brain level or within the BBBO ROI. Although Labriji et al. (2023) reported a 29.6 ± 15.1 % decrease in CBF and prolonged ATT following BBBO in rats (Labriji et al., 2023), our NHP data showed only modest, non-significant fluctuations (whole-brain CBF $\Delta = -3.0$ mL·100 $g^{-1}\cdot min^{-1}$; $p = 0.64$; whole-brain ATT $\Delta = -106.9$ ms; $p = 0.22$). These discrepancies may reflect differences in BBBO targeting and volume, species differences (earlier study in rodents versus our work in non-human primates), and our limited longitudinal sampling, and our lack of longitudinal sampling, which may have missed the critical timeline of CBF drops(Rigollet et al., 2024). In addition,

isoflurane anesthesia, a dose-dependent vasodilator in primates, likely alters CBF and vascular responsiveness during our experiments, further limiting CBF and ATT as reliable, noninvasive biomarkers of BBBO in NHPs (Li et al., 2014).

The study has several limitations. First, the spatial resolution is primarily constrained by the signal-to-noise ratio (SNR), which is influenced by acquisition time and coil sensitivity, and could limit the detection of subtle or spatially heterogeneous permeability changes. Recent motion-compensated, multi-delay diffusion-weighted ASL with isotropic 3.5 mm^3 resolution in humans (Shao et al., 2023) may substantially improve both sensitivity and resolution. Second, DP-pCASL was acquired at approximately 45-60 min post-sonication, capturing only offline effects rather than the full opening–recovery time course. Longitudinal, multi-time point imaging will be essential to elucidate how FUS-BBBO dynamically alters cerebral blood flow and water-exchange metrics over time (Labriji et al., 2023; Rigollet et al., 2024; Sun et al., 2015). Furthermore, our single-pass approximation kinetic model simplifies the microvascular environment and does not fully capture transcellular water movement through AQP4 channels or intra-voxel transit-time heterogeneity. While we accounted for voxel-wise arterial transit time (ATT) in this study, further refinements could incorporate mechanisms suggested by recent multi-echo time ASL studies, such as using varying echo times to probe AQP4-associated transcellular flux (Ohene et al., 2019), or modeling intra-voxel transit-time dispersion to improve estimation accuracy (Mahroo et al., 2021). Incorporating these advanced models and validating the resulting K_w values against dynamic contrast-enhanced MRI–derived K^{trans} measurements (Hývlová et al., 2025; Tiwari et al., 2025; Vlachos et al., 2010) could enable precise mapping of how FUS affects both the timing and spatial distribution of transcellular and paracellular water exchange.

In conclusion, our findings demonstrate that FUS-mediated BBB opening results in decreased K_w at the focal site alongside a global increase in whole-brain K_w, revealing complex physiological adaptations that can be noninvasively monitored using DP-pCASL. This technique offers a safe,

repeatable, and sensitive tool for detecting and tracking BBB permeability changes, with strong potential for both preclinical research and clinical application in neurotherapeutics.

Credit author statement

D.L. and V.P.F. designed the study, collective and analyzed the data and wrote the manuscript. X.S. and D.J.J.W. provided critical support for implementing the DP-pCASL sequences and processing the data. R.L. configured the MRI sequence and assisted with data collection. F.M. and S.S. helped with study design, device calibration, and data collection. E.E.K. provided focused ultrasound expertise. V.P.F. and E.E.K. supervised the study.

Acknowledgements

The authors wish to acknowledge the ZI-ICM team for the setup and anesthesia procedures during MRI imaging, and ZI-MRI team for the MRI sequence setup and data collection. The work was supported by NIH R01 MH133020 (V.P. Ferrera and E.E. Konofagou), R01 NS134712 (D.J. Wang) and BBRF Young Investigator grant 31298 (D. Liu).

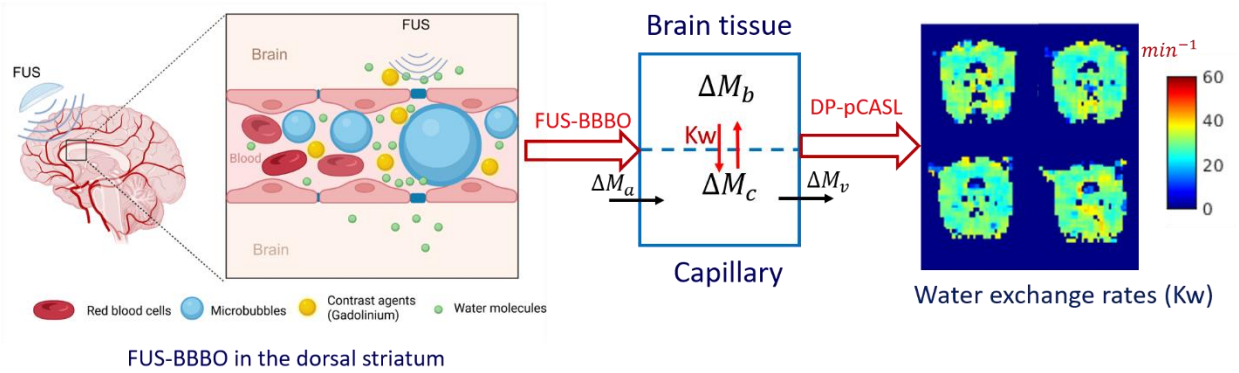

Figure 1 Schematic pipeline for measuring blood–brain barrier (BBB) water exchange between capillary and brain tissue using diffusion-prepared pseudo-continuous arterial spin labeling (DP-pCASL) after focused ultrasound (FUS)–mediated BBB opening in non-human primates (NHPs). Part of the figure was created using BioRender.com.

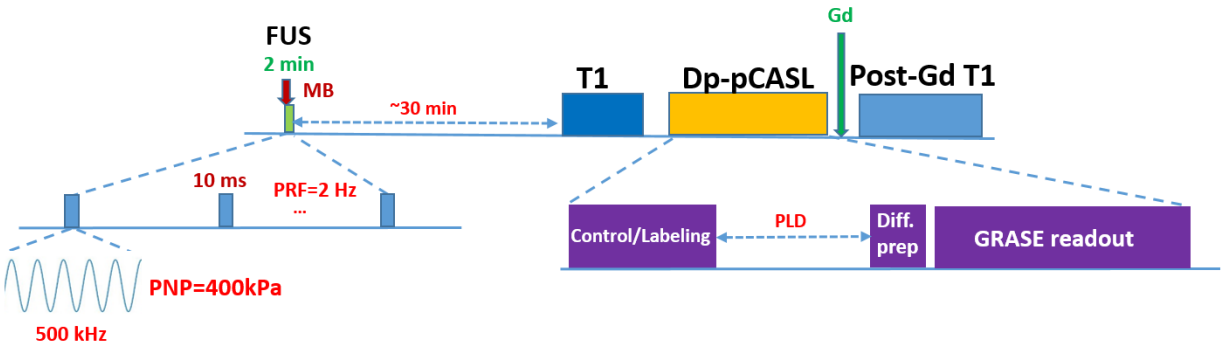

Figure 2 FUS procedures and MRI acquisition: A 2-min focused ultrasound (FUS) exposure combined with microbubbles (MB) was followed by MRI scans, including T1, diffusion-prepared pCASL (2.2 × 2.2 × 5 mm^3 resolution, 600-1700 ms post-labeling delays (PLDs), with diffusion weighted), and a post-Gadolinium T1 scan to confirm blood-brain barrier (BBB) opening.

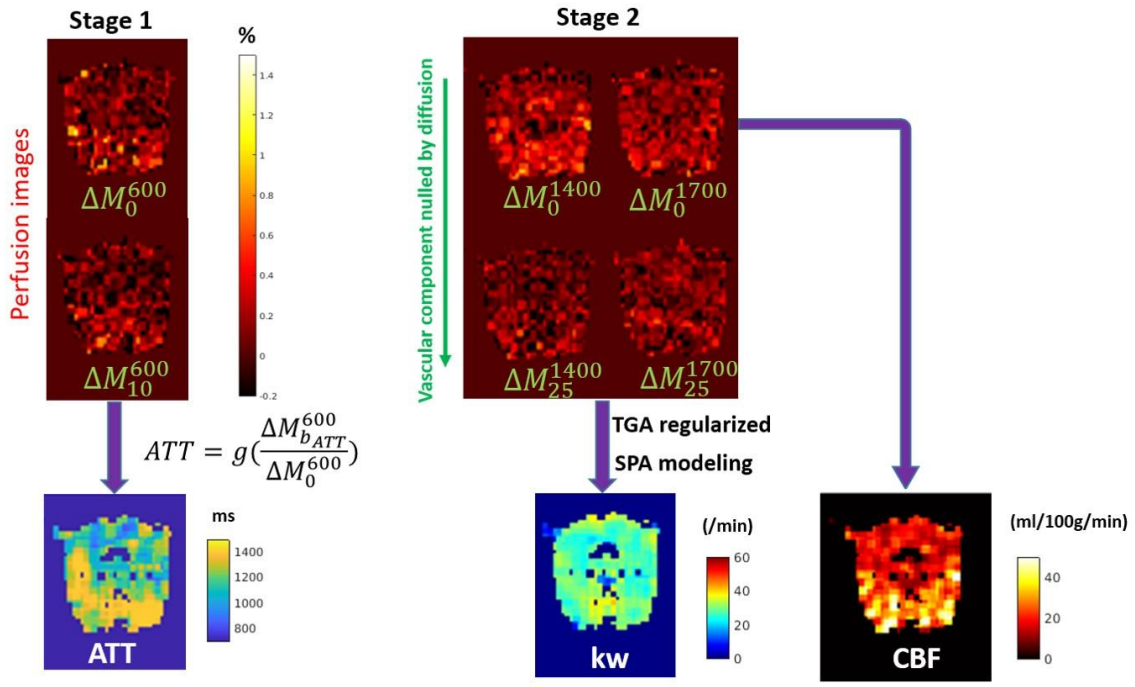

Figure 3 Two-stage estimation of arterial transit time (ATT), water-exchange rate (K_w), and cerebral blood flow (CBF). ATT is estimated via FEAST using the ratio of diffusion-weighted (b_{ATT} = 10 s/mm²) to non-weighted ASL signal at post-labeling delay (PLD) = 600 ms. K_w is derived from the two-compartment single-pass approximation model fitted to DP-pCASL data. CBF is calculated from ΔM_0^{1700} (b = 0 s/mm², PLD = 1700 ms) without diffusion preparation. Here, ΔM_b^{PLD} denotes the ASL difference signal with diffusion weighting b and delay PLD.

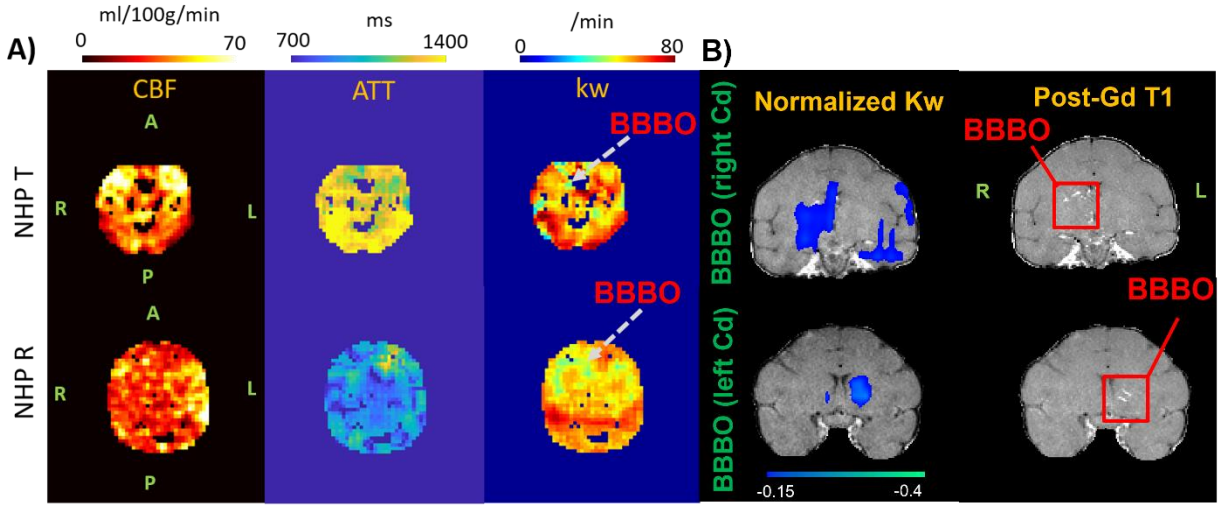

Figure 4 A) Representative maps of cerebral blood flow (CBF), arterial transit time (ATT), and water exchange rate (K_w) from two non-human primates (NHPs R and T) following focused ultrasound (FUS) with microbubbles targeting the right caudate. Color maps are shown in the horizontal plane, with arrows indicating regions of reduced K_w, potentially corresponding to blood-brain barrier opening(BBBO). B) Normalized $K_w$maps (scaled to each brain's maximum K_w and post-Gadolinium T1 images demonstrate ~15–40% reduction in water exchange rates at and around the BBBO site (Top: BBBO in right caudate; Bottom: BBBO in left caudate). R: Right; L: Left; A: Anterior; P: Posterior; S: Superior; I: Inferior.

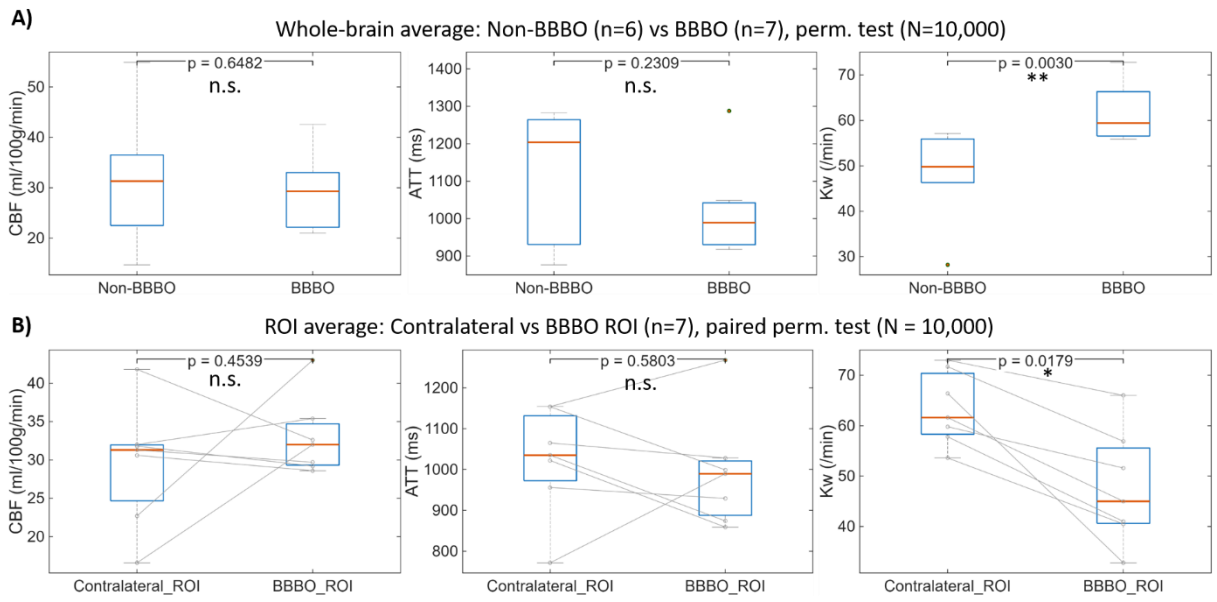

Figure 5 A) Whole-brain averages of cerebral blood flow (CBF), arterial transit time (ATT), and BBB water exchange rate (K_w) in non-BBBO (n = 6 sessions, 4 NHPs) and FUS-BBBO conditions (n = 7 sessions, 4 NHPs). Permutation tests (N = 10,000) showed no significant differences in CBF and ATT ($p > 0.05$), but a significant increase in whole-brain K_w following BBBO ($p < 0.01$). B) ROI analysis comparing the BBBO site (caudate) and the contralateral control region within the same sessions revealed a significant reduction in K_w at the BBBO site ($p < 0.05$, paired permutation test), while CBF and ATT showed no significant differences ($p>0.05$). All box plots display the median, 25th and 75th percentiles (box edges), and individual outliers.

References

Abbott, N.J., Rönnbäck, L., Hansson, E., 2006. Astrocyte–endothelial interactions at the blood–brain barrier. Nature Reviews Neuroscience 7, 41-53.

Alsop, D.C., Detre, J.A., Golay, X., Günther, M., Hendrikse, J., Hernandez‐Garcia, L., Lu, H., MacIntosh, B.J., Parkes, L.M., Smits, M., 2015. Recommended implementation of arterial spin‐labeled perfusion MRI for clinical applications: a consensus of the ISMRM perfusion study group and the European consortium for ASL in dementia. Magnetic resonance in medicine 73, 102-116.

Armulik, A., Genové, G., Betsholtz, C., 2011. Pericytes: developmental, physiological, and pathological perspectives, problems, and promises. Developmental cell 21, 193-215.

Aryal, M., Arvanitis, C.D., Alexander, P.M., McDannold, N., 2014. Ultrasound-mediated blood–brain barrier disruption for targeted drug delivery in the central nervous system. Advanced Drug Delivery Reviews 72, 94-109.

Burgess, A., Shah, K., Hough, O., Hynynen, K., 2015. Focused ultrasound-mediated drug delivery through the blood–brain barrier. Expert review of neurotherapeutics 15, 477-491.

Chen, G., Li, H., Shao, X., Wang, D.J., Hu, W., Han, Y., Yang, Q., 2025. Decreased water exchange rate across the blood–brain barrier throughout the Alzheimer's disease continuum: Evidence from Chinese data. Alzheimer's & Dementia 21, e70089.

Chu, P.-C., Liu, H.-L., Lai, H.-Y., Lin, C.-Y., Tsai, H.-C., Pei, Y.-C., 2015. Neuromodulation accompanying focused ultrasound-induced blood-brain barrier opening. Scientific reports 5, 15477.

Cong, X., Kong, W., 2020. Endothelial tight junctions and their regulatory signaling pathways in vascular homeostasis and disease. Cellular signalling 66, 109485.

Daneman, R., Prat, A., 2015. The blood–brain barrier. Cold Spring Harbor perspectives in biology 7, a020412.

Danieli, L., Riccitelli, G., Distefano, D., Prodi, E., Ventura, E., Cianfoni, A., Kaelin-Lang, A., Reinert, M., Pravatà, E., 2019. Brain tumor-enhancement visualization and morphometric assessment: a comparison of MPRAGE, SPACE, and VIBE MRI techniques. American Journal of Neuroradiology 40, 1140-1148.

Dickie, B.R., Parker, G.J., Parkes, L.M., 2020. Measuring water exchange across the blood-brain barrier using MRI. Progress in Nuclear Magnetic Resonance Spectroscopy 116, 19-39.

Downs, M.E., Teichert, T., Buch, A., Karakatsani, M.E., Sierra, C., Chen, S., Konofagou, E.E., Ferrera, V.P., 2017. Toward a cognitive neural prosthesis using focused ultrasound. Frontiers in Neuroscience 11, 607.

Gulani, V., Calamante, F., Shellock, F.G., Kanal, E., Reeder, S.B., 2017. Gadolinium deposition in the brain: summary of evidence and recommendations. The Lancet Neurology 16, 564-570.

Harvey, H.B., Gowda, V., Cheng, G., 2020. Gadolinium deposition disease: a new risk management threat. Journal of the American College of Radiology 17, 546-550.

Hawkins, B.T., Davis, T.P., 2005. The blood-brain barrier/neurovascular unit in health and disease. Pharmacological reviews 57, 173-185.

Hirt, L., Fukuda, A.M., Ambadipudi, K., Rashid, F., Binder, D., Verkman, A., Ashwal, S., Obenaus, A., Badaut, J., 2017. Improved long-term outcome after transient cerebral ischemia in aquaporin-4 knockout mice. Journal of Cerebral Blood Flow & Metabolism 37, 277-290.

Hynynen, K., McDannold, N., Vykhodtseva, N., Jolesz, F.A., 2001. Noninvasive MR imaging–guided focal opening of the blood-brain barrier in rabbits. Radiology 220, 640-646.

Hývlová, D., Jiřík, R., Vitouš, J., Macíček, O., Krátká, L., Dražanová, E., Starčuk Jr, Z., 2025. Focused ultrasound–induced blood–brain barrier opening: A comparative analysis of permeability quantification based on K trans and PS. Magnetic resonance in medicine 93, 2610-2622.

Jenkinson, M., Beckmann, C.F., Behrens, T.E., Woolrich, M.W., Smith, S.M., 2012. Fsl. Neuroimage 62, 782-790.

Kanda, T., Ishii, K., Kawaguchi, H., Kitajima, K., Takenaka, D., 2014. High signal intensity in the dentate nucleus and globus pallidus on unenhanced T1-weighted MR images: relationship with increasing cumulative dose of a gadolinium-based contrast material. Radiology 270, 834-841.

Karakatsani, M.E., Pouliopoulos, A.N., Liu, M., Jambawalikar, S.R., Konofagou, E.E., 2020. Contrast-free detection of focused ultrasound-induced blood-brain barrier opening using diffusion tensor imaging. IEEE Transactions on Biomedical Engineering 68, 2499-2508.

Konofagou, E.E., 2012. Optimization of the ultrasound-induced blood-brain barrier opening. Theranostics 2, 1223.

Kovacs, Z.I., Kim, S., Jikaria, N., Qureshi, F., Milo, B., Lewis, B.K., Bresler, M., Burks, S.R., Frank, J.A., 2017. Disrupting the blood–brain barrier by focused ultrasound induces sterile inflammation. Proceedings of the National Academy of Sciences 114, E75-E84.

Labriji, W., Clauzel, J., Mestas, J.L., Lafond, M., Lafon, C., Salabert, A.S., Hirschler, L., Warnking, J.M., Barbier, E.L., Loubinoux, I., 2023. Evidence of cerebral hypoperfusion consecutive to ultrasound ‐ mediated blood ‐ brain barrier opening in rats. Magnetic resonance in medicine 89, 2281-2294.

Le Bihan, D., Iima, M., 2015. Diffusion magnetic resonance imaging: what water tells us about biological tissues. PLoS biology 13, e1002203.

Leinenga, G., Langton, C., Nisbet, R., Götz, J., 2016. Ultrasound treatment of neurological diseases—current and emerging applications. Nature Reviews Neurology 12, 161-174.

Li, C.-X., Patel, S., Wang, D.J., Zhang, X., 2014. Effect of high dose isoflurane on cerebral blood flow in macaque monkeys. Magnetic resonance imaging 32, 956-960.

Li, Y., Sadiq, A., Wang, Z., 2022. Arterial spin labelling-based blood-brain barrier assessment and its applications. Investigative magnetic resonance imaging 26, 229.

Li, Y., Ying, Y., Yao, T., Jia, X., Liang, H., Tang, W., Jia, X., Song, H., Shao, X., Wang, D.J., 2023. Decreased water exchange rate across blood–brain barrier in hereditary cerebral small vessel disease. Brain 146, 3079-3087.

Lipsman, N., Meng, Y., Bethune, A.J., Huang, Y., Lam, B., Masellis, M., Herrmann, N., Heyn, C., Aubert, I., Boutet, A., 2018. Blood–brain barrier opening in Alzheimer's disease using MR-guided focused ultrasound. Nature communications 9, 2336.

Liu, D., Munoz, F., Sanatkhani, S., Pouliopoulos, A.N., Konofagou, E.E., Grinband, J., Ferrera, V.P., 2023. Alteration of functional connectivity in the cortex and major brain networks of non-human primates following focused ultrasound exposure in the dorsal striatum. Brain stimulation 16, 1196-1204.

Mahroo, A., Buck, M.A., Huber, J., Breutigam, N.-J., Mutsaerts, H.J., Craig, M., Chappell, M., Günther, M., 2021. Robust multi-TE ASL-based blood–brain barrier integrity measurements. Frontiers in Neuroscience 15, 719676.

Mainprize, T., Lipsman, N., Huang, Y., Meng, Y., Bethune, A., Ironside, S., Heyn, C., Alkins, R., Trudeau, M., Sahgal, A., 2019. Blood-brain barrier opening in primary brain tumors with non-invasive MR-guided focused ultrasound: a clinical safety and feasibility study. Scientific reports 9, 321.

Marquet, F., Teichert, T., Wu, S.-Y., Tung, Y.-S., Downs, M., Wang, S., Chen, C., Ferrera, V., Konofagou, E.E., 2014. Real-time, transcranial monitoring of safe blood-brain barrier opening in non-human primates. PloS one 9, e84310.

McDannold, N., Vykhodtseva, N., Hynynen, K., 2006. Targeted disruption of the blood–brain barrier with focused ultrasound: association with cavitation activity. Physics in Medicine & Biology 51, 793.

McDannold, N., Vykhodtseva, N., Hynynen, K., 2007. Use of ultrasound pulses combined with Definity for targeted blood-brain barrier disruption: a feasibility study. Ultrasound in medicine & biology 33, 584-590.

McMahon, D., Hynynen, K., 2017. Acute inflammatory response following increased blood-brain barrier permeability induced by focused ultrasound is dependent on microbubble dose. Theranostics 7, 3989.

Meng, Y., MacIntosh, B.J., Shirzadi, Z., Kiss, A., Bethune, A., Heyn, C., Mithani, K., Hamani, C., Black, S.E., Hynynen, K., 2019. Resting state functional connectivity changes after MR-guided focused ultrasound mediated blood-brain barrier opening in patients with Alzheimer's disease. Neuroimage 200, 275-280.

Mestre, H., Hablitz, L.M., Xavier, A.L., Feng, W., Zou, W., Pu, T., Monai, H., Murlidharan, G., Castellanos Rivera, R.M., Simon, M.J., 2018. Aquaporin-4-dependent glymphatic solute transport in the rodent brain. Elife 7, e40070.

Ohene, Y., Harrison, I.F., Nahavandi, P., Ismail, O., Bird, E.V., Ottersen, O.P., Nagelhus, E.A., Thomas, D.L., Lythgoe, M.F., Wells, J.A., 2019. Non-invasive MRI of brain clearance pathways using multiple echo time arterial spin labelling: an aquaporin-4 study. Neuroimage 188, 515-523.

Palomares, J.A., Tummala, S., Wang, D.J., Park, B., Woo, M.A., Kang, D.W., Lawrence, K.S.S., Harper, R.M., Kumar, R., 2015. Water exchange across the blood ‐ brain barrier in obstructive sleep apnea: An MRI diffusion ‐ weighted pseudo ‐ continuous arterial spin labeling study. Journal of neuroimaging 25, 900-905.

Papadopoulos, M.C., Verkman, A.S., 2013. Aquaporin water channels in the nervous system. Nature Reviews Neuroscience 14, 265-277.

Pappas, C., Bauer, C.E., Zachariou, V., Maillard, P., Caprihan, A., Shao, X., Wang, D.J., Gold, B.T., 2024. MRI free water mediates the association between water exchange rate across the blood brain barrier and executive function among older adults. Imaging Neuroscience 2, 1-15.

Pouliopoulos, A.N., Kwon, N., Jensen, G., Meaney, A., Niimi, Y., Burgess, M.T., Ji, R., McLuckie, A.J., Munoz, F.A., Kamimura, H.A., 2021. Safety evaluation of a clinical focused ultrasound system for neuronavigation guided blood-brain barrier opening in non-human primates. Scientific reports 11, 15043.

Rezai, A.R., Ranjan, M., D'Haese, P.-F., Haut, M.W., Carpenter, J., Najib, U., Mehta, R.I., Chazen, J.L., Zibly, Z., Yates, J.R., 2020. Noninvasive hippocampal blood− brain barrier opening in

Alzheimer's disease with focused ultrasound. Proceedings of the National Academy of Sciences 117, 9180-9182.

Rigollet, S., Rome, C., Ador, T., Dumont, E., Pichon, C., Delalande, A., Barbier, E.L., Stupar, V., 2024. FUS-mediated BBB opening leads to transient perfusion decrease and inflammation without acute or chronic brain lesion. Theranostics 14, 4147.

Shao, X., Jann, K., Ma, S.J., Yan, L., Montagne, A., Ringman, J.M., Zlokovic, B.V., Wang, D.J., 2020. Comparison between blood-brain barrier water exchange rate and permeability to gadolinium-based contrast agent in an elderly cohort. Frontiers in Neuroscience 14, 571480.

Shao, X., Ma, S.J., Casey, M., D' Orazio, L., Ringman, J.M., Wang, D.J., 2019. Mapping water exchange across the blood‐brain barrier using 3D diffusion‐prepared arterial spin labeled perfusion MRI. Magnetic resonance in medicine 81, 3065-3079.

Shao, X., Shou, Q., Felix, K., Ojogho, B., Jiang, X., Gold, B.T., Herting, M.M., Goldwaser, E.L., Kochunov, P., Hong, E., 2024. Age-related decline in blood-brain barrier function is more pronounced in males than females in parietal and temporal regions. Elife 13, RP96155.

Shao, X., Zhao, C., Shou, Q., St Lawrence, K.S., Wang, D.J., 2023. Quantification of blood‐brain barrier water exchange and permeability with multidelay diffusion‐weighted pseudo‐continuous arterial spin labeling. Magnetic resonance in medicine 89, 1990-2004.

Sheikov, N., McDannold, N., Vykhodtseva, N., Jolesz, F., Hynynen, K., 2004. Cellular mechanisms of the blood-brain barrier opening induced by ultrasound in presence of microbubbles. Ultrasound in medicine & biology 30, 979-989.

Sourbron, S.P., Buckley, D.L., 2013. Classic models for dynamic contrast‐enhanced MRI. NMR in Biomedicine 26, 1004-1027.

St. Lawrence, K.S., Owen, D., Wang, D.J., 2012. A two‐stage approach for measuring vascular water exchange and arterial transit time by diffusion‐weighted perfusion MRI. Magnetic resonance in medicine 67, 1275-1284.

Sun, T., Samiotaki, G., Wang, S., Acosta, C., Chen, C.C., Konofagou, E.E., 2015. Acoustic cavitation-based monitoring of the reversibility and permeability of ultrasound-induced blood-brain barrier opening. Physics in Medicine & Biology 60, 9079.

Sweeney, M.D., Zhao, Z., Montagne, A., Nelson, A.R., Zlokovic, B.V., 2018. Blood-brain barrier: from physiology to disease and back. Physiological reviews.

Tang, G., Liu, Y., Zhang, Z., Lu, Y., Wang, Y., Huang, J., Li, Y., Chen, X., Gu, X., Wang, Y., 2014. Mesenchymal stem cells maintain blood-brain barrier integrity by inhibiting aquaporin-4 upregulation after cerebral ischemia. Stem Cells 32, 3150-3162.

Tiwari, Y.V., Muir, E.R., Jiang, Z., Duong, T.Q., 2025. Diffusion-weighted arterial spin labeling MRI to investigate mannitol-induced blood brain barrier disruption. Magnetic resonance imaging, 110335.

Todd, N., Zhang, Y., Arcaro, M., Becerra, L., Borsook, D., Livingstone, M., McDannold, N., 2018. Focused ultrasound induced opening of the blood-brain barrier disrupts inter-hemispheric resting state functional connectivity in the rat brain. Neuroimage 178, 414-422.

Todd, N., Zhang, Y., Livingstone, M., Borsook, D., McDannold, N., 2019. The neurovascular response is attenuated by focused ultrasound-mediated disruption of the blood-brain barrier. Neuroimage 201, 116010.

Tung, Y.-S., Marquet, F., Teichert, T., Ferrera, V., Konofagou, E.E., 2011. Feasibility of noninvasive cavitation-guided blood-brain barrier opening using focused ultrasound and microbubbles in nonhuman primates. Applied physics letters 98.

Uchida, Y., Kan, H., Sakurai, K., Oishi, K., Matsukawa, N., 2023. Contributions of blood–brain barrier imaging to neurovascular unit pathophysiology of Alzheimer's disease and related dementias. Frontiers in Aging Neuroscience 15, 1111448.

Vlachos, F., Tung, Y., Konofagou, E., 2010. Permeability assessment of the focused ultrasound-induced blood–brain barrier opening using dynamic contrast-enhanced MRI. Physics in Medicine & Biology 55, 5451.

Wang, J., Alsop, D.C., Song, H.K., Maldjian, J.A., Tang, K., Salvucci, A.E., Detre, J.A., 2003. Arterial transit time imaging with flow encoding arterial spin tagging (FEAST). Magnetic Resonance in Medicine: An Official Journal of the International Society for Magnetic Resonance in Medicine 50, 599-607.

Wang, J., Fernández-Seara, M.A., Wang, S., Lawrence, K.S.S., 2007. When perfusion meets diffusion: in vivo measurement of water permeability in human brain. Journal of Cerebral Blood Flow & Metabolism 27, 839-849.

Wengler, K., Ha, J., Syritsyna, O., Bangiyev, L., Coyle, P.K., Duong, T.Q., Schweitzer, M.E., He, X., 2020. Abnormal blood-brain barrier water exchange in chronic multiple sclerosis lesions: A preliminary study. Magnetic resonance imaging 70, 126-133.

Xu, X., Chan, K.W., Knutsson, L., Artemov, D., Xu, J., Liu, G., Kato, Y., Lal, B., Laterra, J., McMahon, M.T., 2015. Dynamic glucose enhanced (DGE) MRI for combined imaging of blood–brain barrier break down and increased blood volume in brain cancer. Magnetic resonance in medicine 74, 1556-1563.

Zeppenfeld, D.M., Simon, M., Haswell, J.D., D'Abreo, D., Murchison, C., Quinn, J.F., Grafe, M.R., Woltjer, R.L., Kaye, J., Iliff, J.J., 2017. Association of perivascular localization of aquaporin-4 with cognition and Alzheimer disease in aging brains. JAMA neurology 74, 91-99.